Macromolecules

pubs.acs.org/Macromolecules Article

Polyelectrolyte Complex-Covalent Interpenetrating Polymer Network Hydrogels

Defu Li, Tobias Göckler, Ute Schepers, and Samanvaya Srivastava*

Cite This: *Macromolecules* 2022, 55, 4481−4491 Read Online

ACCESS | Metrics & More | Article Recommendations | Supporting Information

ABSTRACT: Polyelectrolyte complex (PEC) hydrogels possess rich microstructural diversity and tunability of the shear response, self-healing attributes, and pH- and salt-responsiveness. Yet, their utility in biotechnology and biomedicine has been limited, owing to their weak mechanical strength and uncontrolled swelling. Here, we introduce a strategy to overcome these drawbacks of PEC hydrogels by interlacing the electrostatically crosslinked PEC network with a covalently crosslinked polymer network, creating polyelectrolyte complex-covalent interpenetrating polymer network (PEC-IPN) hydrogels. Structural and material characterizations of model PEC-IPN hydrogels composed of oppositely charged *ABA* triblock copolymers and photocrosslinkable 4-arm poly(ethylene oxide) (PEO) highlight the key advantages of our approach. Upon initial mixing of the three constituents, the PEC network self-assembles swiftly in aqueous environs, providing structural rigidity and serving as protective scaffoldings for the covalently crosslinkable PEO precursors. Photocrosslinking of the PEO chains creates a covalent network, providing structural reinforcement to the PEC network. The resulting PEC-IPN hydrogels possess significantly improved shear and tensile strengths, swelling characteristics, and mechanical stability in saline environments while preserving the intrinsic mesoscale structure of the PEC network and its salt-responsiveness. We envision that our approach to fabricating PEC-based IPN hydrogels will pave the way for the creation of self-assembled hybrid materials that harness the unique attributes of electrostatic self-assembly pathways, with broad applications in biomedicine.

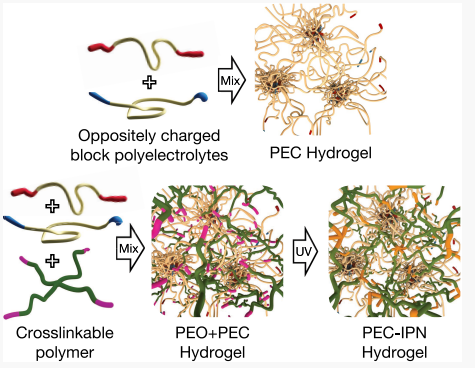

1. INTRODUCTION

Polyelectrolyte complex (PEC) hydrogels[1−12] present an exciting platform for the development of soft materials that cater to diverse applications in biomedicine[13,14] as scaffolds for tissue engineering,[15−18] bioadhesives,[19−26] and drug delivery;[27−31] as ionic conductors;[32,33] and in food industries.[34,35] These hydrogels self-assemble rapidly[1,9] upon mixing aqueous solutions of oppositely charged block polyelectrolytes and exhibit hierarchical microstructures,[4,5,36−39] comprising three-dimensional networks of PEC domains (composed of the oppositely charged blocks) connected to each other *via* the neutral blocks. This microstructure differentiates PEC hydrogels from ionically crosslinked hydrogels[40−47] (typically composed of homopolyelectrolytes) and contributes to their unique combination of attributes, including tunable shear properties,[2,4−6,9,12,48] stimuli (salt- and pH-) responsiveness,[1,2,4,8,9,48] injectability,[12,49] self-healing properties,[12,49] and the ability to encapsulate charged macromolecules such as proteins and nucleic acids.[50−54]

Yet, broad applications of PEC hydrogels remain limited owing to their physical crosslinked structure contributing to low shear strength (typically less than 20 kPa), miniscule tensile strength, and an inherent coupling between the network microstructure and its shear response.[5] In contrast, applications such as tissue adhesion typically require hydrogel sealants to mimic the shear properties of the tissue substrates (e.g., ∼1 kPa for soft tissue, ∼10 kPa for muscle, ∼50 kPa for skin, and >100 kPa for cartilage and bone).[55−57] At the same time, PEC hydrogels swell indefinitely and eventually dissolve upon exposure to aqueous media, indicating degradation of the hydrogel structure.[3,58] Limited and tunable swelling can avoid material loss, preserve the stability of structure and mechanical properties, and maintain the functions of PEC hydrogels which can broaden their utility. However, effective measures for controlling the swelling of PEC hydrogels remain elusive.

Here, we introduce a strategy to address these shortcomings of PEC hydrogels while retaining their unique attributes by interlacing the PEC network with a covalent network. Interpenetration of polymer networks has been employed to imbue properties like toughness and stimuli-responsiveness in hydrogels.[59−64] In this work, we demonstrate synergic improvements in the material properties of PEC-covalent interpenetrating polymer network (IPN) hydrogels which are not accessible in hydrogels composed of either of the two

Received: March 22, 2022
Revised: May 6, 2022
Published: June 2, 2022

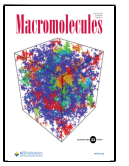

https://doi.org/10.1021/acs.macromol.2c00590
Macromolecules 2022, 55, 4481−4491

networks, including substantial improvements in mechanical strength, toughness, and swelling performance while conserving the microstructure of the PEC network. Moreover, our approach offers a strategy to expand the utility of photocrosslinkable hydrogels by enabling *in situ* crosslinking of the photocrosslinkable precursor polymers. The self-assembled PEC hydrogels provide a protective environment for the photocrosslinkable precursors, mitigating dilution and deactivation prior to their crosslinking. We envision that the PEC-covalent IPN platform demonstrated here will constitute the first steps toward the implementation of PEC-based IPN hydrogels in future biomedical applications.

2. MATERIALS AND METHODS

2.1. Materials. Potassium (99.5% trace metals basis), naphthalene, poly(ethylene glycol) (M_n = 20,000 Da), 2,2-dimethoxy-2-phenylacetophenone, allyl glycidyl ether (AGE), calcium hydride, sodium 3-mercapto-1-propanesulfonate, technical grade (90%), 1*H*-pyrazole-1-carboxamidine hydrochloride (99%), cysteamine hydrochloride (≥98%), and Irgacure 2959 were obtained from Millipore Sigma. Tetrahydrofuran (THF) and dimethylformamide (DMF) were obtained from Fisher Scientific. 4-Arm poly(ethylene oxide) acrylate (PEO, M_n = 20,000 Da, ≥ 95%) was obtained from JenKem Technology.

2.2. Block Polyelectrolyte Synthesis. Guanidinium, ammonium, and sulfonate functionalized poly(ally glycidyl ether)-*b*-poly(ethylene glycol)-*b*-poly(ally glycidyl ether) were synthesized following previously published protocols.[1] Briefly, AGE was purified by stirring with calcium hydride overnight and then processed by three freeze−pump−thaw cycles and distillation. Poly(ethylene glycol) (M_n = 20,000 Da) was dissolved in anhydrous THF and titrated with potassium naphthalenide (0.4 M in anhydrous THF) until the solution acquired a light green color. AGE was added to the reaction mixture and stirred at 45 °C for 48 h. The polymerization reaction was terminated by the addition of degassed methanol, and the final product poly(allyl glycidyl ether)−poly(ethylene glycol)−poly(allyl glycidyl ether) (PAGE−PEO−PAGE) was precipitated in hexane and filtered, followed by drying prior to further functionalization. The product was characterized by proton nuclear magnetic resonance (^{1}H NMR, 400 MHz), as shown in Figure S1. The degree of polymerization of the PAGE blocks was calculated from the relative heights of peaks in the NMR spectra and was determined to be $PAGE_{98}$−PEO_{455}−$PAGE_{98}$.

The thiol−ene reactions were carried out by dissolving 2 g $PAGE_{98}$−PEO_{455}−$PAGE_{98}$ polymer and a functional thiol (5 equiv per alkene) in a 30 mL DMF/water mixture with a 1:1 volume ratio in a 100 mL round bottom flask. Cysteamine hydrochloride and sodium 3-mercapto-1-propanesulfonate were used to functionalize the block polymers with ammonium and sulfonate groups, respectively. After the addition of the photoinitiator (2,2-dimethoxy-2-phenylacetophenone, 0.05 equiv per alkene), the solution was irradiated with UV light (365 nm) for 6 h under a nitrogen atmosphere. Then, the final product solution was dialyzed against deionized water for 10 cycles of 8 h each. The final ammonium or sulfonate functionalized polymers were obtained by lyophilization.[1,5]

The guanidinium functionalized polymer was synthesized by dissolving ∼2 g of ammonium functionalized $PAGE_{98}$−PEO_{455}−$PAGE_{98}$ in 200 mL of phosphate-buffered saline (PBS) solution along with 1*H*-pyrazole-1-carboxamidine (4 equivalent per amine). The pH of the solution was adjusted to 10 by using 10 M NaOH solution. The reaction mixture was stirred for 3 days, followed by dialysis against deionized water for 10 cycles of 8 h each. The final guanidinium functionalized polymers were obtained by lyophilization. All functionalized products were characterized by ^{1}H NMR (400 MHz) (Figure S1).[1,5]

2.3. Preparation of PEC, PEC + PEO, and PEC−IPN Hydrogels. 50 wt % stock solutions of the cationic and anionic block polyelectrolytes were prepared by mixing, for example, 500 mg of the polymers with 1 mL of deionized water. PEC hydrogels were prepared by mixing an appropriate amount of block polycation stock solution with deionized water. Then, an appropriate amount of the block polyanion stock solution was added to the solution. Vortex mixing was carried out for 15 s to ensure homogenous mixing. The polymers were mixed in proportions such that the molar charge ratio of cationic and anionic groups was 1:1.

PEC + PEO hydrogels were prepared by mixing the block polycation stock solution with an aqueous solution of PEO and photoinitiator Irgacure 2959. Subsequently, the block polyanion stock solution was added. Each addition step was followed by vortex mixing for 15 s to homogenize the mixtures. The polymers were mixed in proportions such that the molar charge ratio of cationic and anionic groups was 1:1.

PEC−IPN hydrogels were prepared by exposing PEC + PEO hydrogels to UV radiation (302 nm, 8 W) for 5 min. The hydrogels were subjected to further characterization as is, without further purification or removal of unreacted PEO chains.

2.4. Small-Angle X-Ray Scattering Measurement. Small-angle X-ray scattering (SAXS) measurements were performed at beamline 12-ID-B at the Advanced Photon Source, Argonne National Laboratory with 13 keV X-rays. The sample-to-detector distance was set at 4 m, corresponding to a wave vector (q) range of 0.0002 to 0.5 Å^{-1}. PEC and PEC + PEO hydrogels were loaded into holes (3 mm diameter) in 4 mm thick aluminum strips using a positive displacement pipette and sealed on both sides with Kapton tape to avoid water evaporation. PEC−IPN hydrogels were prepared by loading PEC + PEO hydrogels in the aluminum strips and followed by 5 min UV light exposure and then sealed by Kapton tape. All the samples were prepared and loaded onto the sample holders at least 24 h before the SAXS measurements. All experiments were performed at room temperature. The X-ray exposure time was set at 0.1 s. The two-dimensional scattering data were converted into one-dimensional data (I_{sample}) by using the matSAXS package. Sample scattering intensity was acquired by subtracting the appropriately scaled background (solvent) scattering intensity ($I_{solvent}$) from the measured scattering intensity, $I(q) = I_{sample} - \alpha I_{solvent}$, with α being the scaling parameter.[5] $P(q)$ and $S(q)$ fits to the $I(q)$ data were carried out using the Irena package[65] in Igor Pro.

2.5. Rheological Measurements. Oscillatory rheological measurements were performed on an Anton Paar MCR 302 rheometer using a parallel plate (diameter: 8 mm, gap size: 0.7 mm) fixture for PEC−IPN hydrogels and a cone and plate (diameter: 10 mm, cone angle: 2°) fixture for PEC and PEC + PEO hydrogels. An appropriate amount of PEC or PEC + PEO hydrogel samples was placed on the lower plate, and excess sample volume was trimmed after reaching the appropriate gap between the cone and the plate. PEC−IPN hydrogel samples were prepared by pipetting 70 μL of PEC + PEO hydrogels into a cylindrical polydimethylsiloxane (PDMS) mold (diameter: 8 mm, height: 1.5 mm) and irradiating the hydrogels with UV radiation for 5 min. The crosslinked hydrogel samples thus obtained were placed between the parallel plates of the rheometer fixture. The hydrogel samples were subjected to small-amplitude oscillatory strain (ω = 1 Hz, γ = 0.3%) for an extended period (1800 s) to equilibrate the samples. Amplitude sweeps, with strain amplitude γ ranging from 0.01−100% (Figure S2) were carried out at frequency ω = 1 rad/s to assess the linear viscoelastic (LVE) regime. Frequency sweeps (ω = 0.01−100 Hz) were performed at γ = 0.3%, staying within the LVE regime. A solvent trap was employed to minimize water evaporation. All rheology data were acquired at 25 °C.

2.6. Tensile Tests. Tensile measurements were conducted on an Instron 5542 mechanical tester. PEO and PEC-IPN hydrogels were prepared by pipetting 80 μL of the precursor solution into a rectangular PDMS mold (12 mm × 5 mm × 1.5 mm) and exposed to UV radiation for photocrosslinking. The crosslinked hydrogels were affixed to the machine tension grips with double-sided tape. The extension rate was set to 1 mm/min, and the stress−strain data were continuously collected until the fracture of samples. The tensile properties were estimated by averaging data obtained from at least 3 hydrogel samples.

https://doi.org/10.1021/acs.macromol.2c00590
Macromolecules 2022, 55, 4481−4491

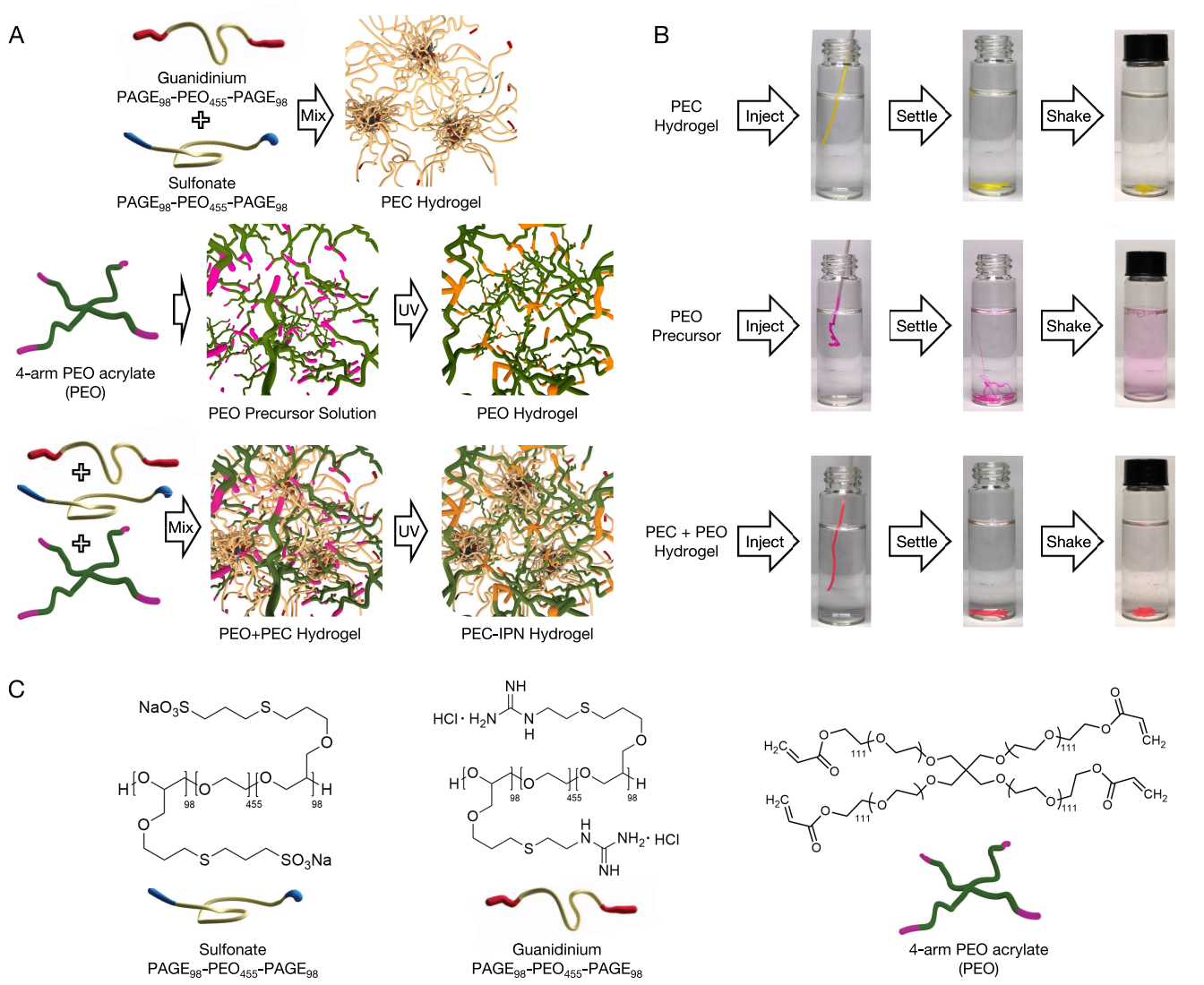

Figure 1. Schematic depiction of PEC, PEC + PEO, and PEC−IPN hydrogels. (A) Schematics representing PEC (row 1), PEO (row 2), and PEC + PEO and PEC-IPN hydrogels (row 3). (B) Photographs demonstrating injectability and insolubility of PEC (row 1) and PEC + PEO (row 3) hydrogels in water. In contrast, the PEO precursor (row 2) dissolves in water readily. Dyes (Acid Yellow 73, Rhodamine B, and a combination of Acid Yellow 73 and Rhodamine B in rows 1, 2, and 3, respectively) were added to the hydrogels to aid visualization. (C) Chemical structures of the block polyelectrolytes and the 4-arm PEO acrylate.

2.7. Swelling Ratio. PEO and PEC−IPN hydrogel samples were prepared by pipetting 60 μL of precursor solution (PEO solution or PEC + PEO hydrogels) into a cylindrical PDMS mold (diameter: 5 mm, height: 3 mm) and irradiating it with UV radiation for 5 min. After UV exposure, the hydrogel samples were transferred into a 24-well culture plate filled with deionized water. After 0, 1, 4, 9, 24, and 48 h, the hydrogel samples were weighed after carefully removing residual water from the surface. The swelling ratio of hydrogels was calculated as

$$\text{swelling ratio} = \frac{m_t}{m_0} \times 100\%$$

Here m_t is the weight of the hydrogel at time t (hour), m_0 is the initial weight. The swelling ratio was calculated by averaging the data of at least 3 samples.

3. RESULTS AND DISCUSSION

3.1. Self-Assembled PEC Networks as Protective Scaffoldings for Covalent Crosslinkable Polymers. PEC hydrogels self-assemble swiftly (≲500 ms)[66−69] upon mixing aqueous solutions of oppositely charged block polyelectrolytes (bPEs) based on $PAGE_{98}$−PEO_{455}−$PAGE_{98}$. The PAGE blocks were functionalized with ionic (guanidinium and sulfonate) moieties[1] (Figure 1A, row 1). These hydrogels are injectable and remain insoluble in water, even upon shaking for a few minutes (Figure 1B, row 1, see also Supporting Information Movie S1).

The introduction of hydrophilic chemically crosslinkable PEO did not impede the PEC gel formation, resulting in injectable PEC + PEO hydrogels (Figure 1A, row 3). The electrostatically self-assembled PEC networks provide structural stability and insolubility in aqueous environments to the PEC + PEO hydrogels (Figure 1B, row 3, see also Supporting Information Movie S2). Moreover, the PEC networks serve as scaffoldings to protect the PEO precursors against uncontrolled dilution (Figure 1B, row 3). Ultraviolet (UV) irradiation of the PEC + PEO hydrogels for 5 min resulted in the formation of polyelectrolyte complex-interpenetrating polymer networks (PEC−IPN) hydrogels composed of water-

https://doi.org/10.1021/acs.macromol.2c00590
Macromolecules 2022, 55, 4481−4491

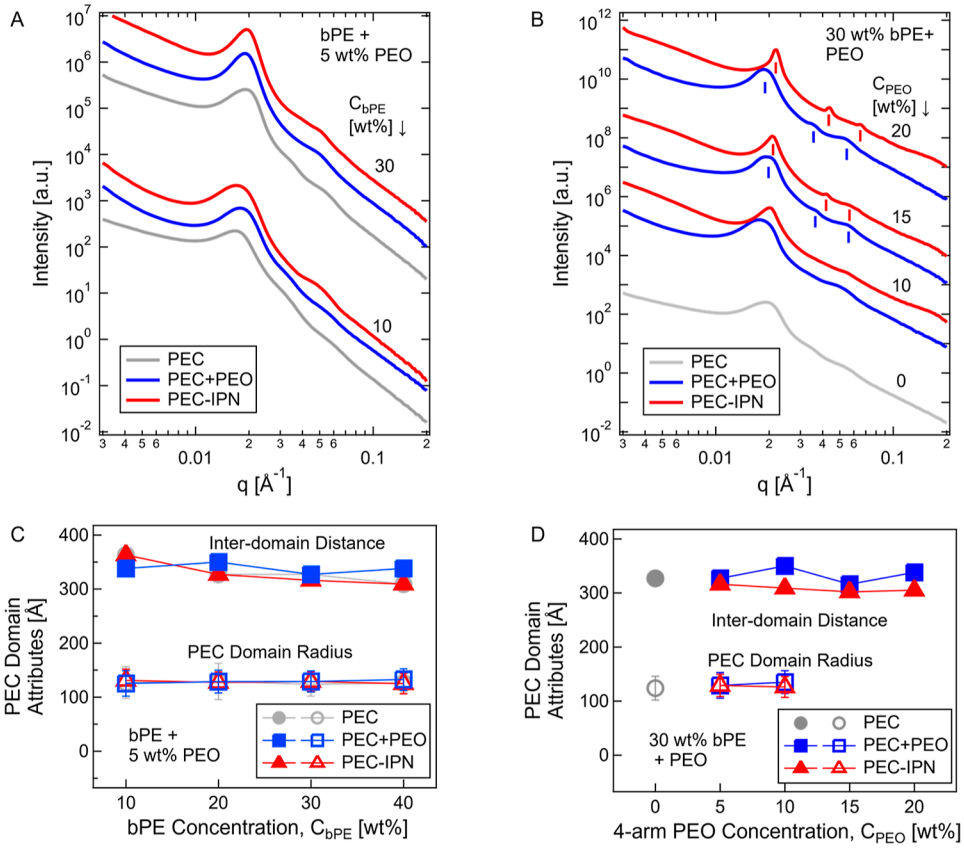

Figure 2. Representative SAXS scattering spectra and PEC domain attributes in PEC, PEC + PEO, and PEC−IPN hydrogels. (A) One-dimensional scattering intensity $I(q)$ as a function of wave vector q for PEC (grey), PEC + PEO (blue), and PEC−IPN (red) hydrogels with varying C_{bPE} from 10 to 30 wt %. PEC + PEO, and PEC−IPN hydrogels also contained a constant C_{PEO} (= 5 wt %). (B) $I(q)$ spectra for PEC hydrogels with C_{bPE} = 30 wt %, and PEC + PEO, and PEC−IPN hydrogels with varying C_{PEO} (between 10 and 20 wt %) and constant C_{bPE} = 30 wt %. In the SAXS spectra for PEC + PEO and PEC−IPN hydrogels with C_{PEO} = 15 and 20 wt %, the small vertical bars indicate the positions of the Bragg scattering peaks. The secondary and the tertiary peaks appear at $2q^*$ and $3q^*$ with respect to the primary peak at q^*, denoting the lamellar microstructure of the PEC domains. In both (A,B), $I(q)$ spectra are shifted vertically for clarity. (C,D) Interdomain distance (d_{PEC}) and domain radius (R_{PEC}) as a function of C_{bPE} (C) and C_{PEO} (D) for PEC, PEC + PEO, and PEC−IPN hydrogels. In (C), C_{PEO} = 5 wt % while in (D), C_{bPE} = 30 wt %. The filled and open symbols referred to the interdomain distance and PEC domain radius, respectively. See Supporting Information Table S1 for peak assignments in (B).

laden interlaced PEC and chemically crosslinked PEO networks (Figure 1A, row 3). In stark contrast, exposure of the solution of crosslinkable polymer precursors to aqueous environments prior to UV-induced crosslinking resulted in rapid dilution of the precursors, limiting their ability to form chemically crosslinked hydrogels (Figure 1A,B, row 2, see also Supporting Information Movie S3).

3.2. Structural Resilience of PEC Domains Against the Inclusion of Polymers and Covalent Networks. SAXS reveals the structural attributes of the PEC network comprising PEC domains interlinked with the neutral blocks of the bPEs. The PEC domains are composed of the charged blocks of the bPEs that possess higher polymer concentration than the surroundings and include higher atomic number elements including nitrogen and sulfur, providing sufficient electron density contrast.[1,4,5] Figure 2A shows representative one-dimensional SAXS intensity $I(q)$ as a function of wave vector q obtained from PEC hydrogels with increasing bPE concentrations (C_{bPE}, grey traces, see also Figure S3A). These SAXS spectra exhibit a broad primary peak near q = 0.02 Å^{-1} followed by secondary peaks at higher q values. The primary and secondary peaks became more prominent with increasing C_{bPE}, indicating strengthening spatial correlations among the PEC domains. Yet, an absence of Bragg reflection peaks denotes that the PEC domains remained in a disordered arrangement even in PEC hydrogels with C_{bPE} = 40 wt %.[1,4,5]

Modeling $I(q)$ as a combination of a form factor $P(q)$ for polydisperse spheres and a hard-sphere structure factor $S(q)$ as $I(q) \sim P(q)S(q)$, as shown in Figure S4, enabled estimation of the domain radius (R_{PEC}) and the characteristic interdomain distance (d_{PEC}).[70,71] The position of the primary $S(q)$ peak, q^*, represents the inverse interdomain distance d_{PEC} as $d_{PEC} \sim 2\pi/q^*$.[70] R_{PEC} and d_{PEC} for the PEC hydrogels are shown in Figure 2C with grey symbols. Consistent with the previous observations[5] that PEC domain size depends on the length of the charged block only, while interdomain correlation and distances are dictated by lengths of both the charged and the neutral blocks as well as C_{bPE}, R_{PEC} was found to be independent of C_{bPE}, while d_{PEC} decreased progressively with increasing C_{bPE}.

Scattering from the PEC network persisted upon the inclusion of polymeric additives (PEO) and their subsequent crosslinking. Figure 2A highlights the similarity of the $I(q)$ spectra obtained from PEC hydrogels (grey traces) with PEC + PEO and PEC−IPN hydrogels containing 5 wt % PEO content (C_{PEO}), depicted by blue and red traces, respectively

https://doi.org/10.1021/acs.macromol.2c00590
Macromolecules 2022, 55, 4481−4491

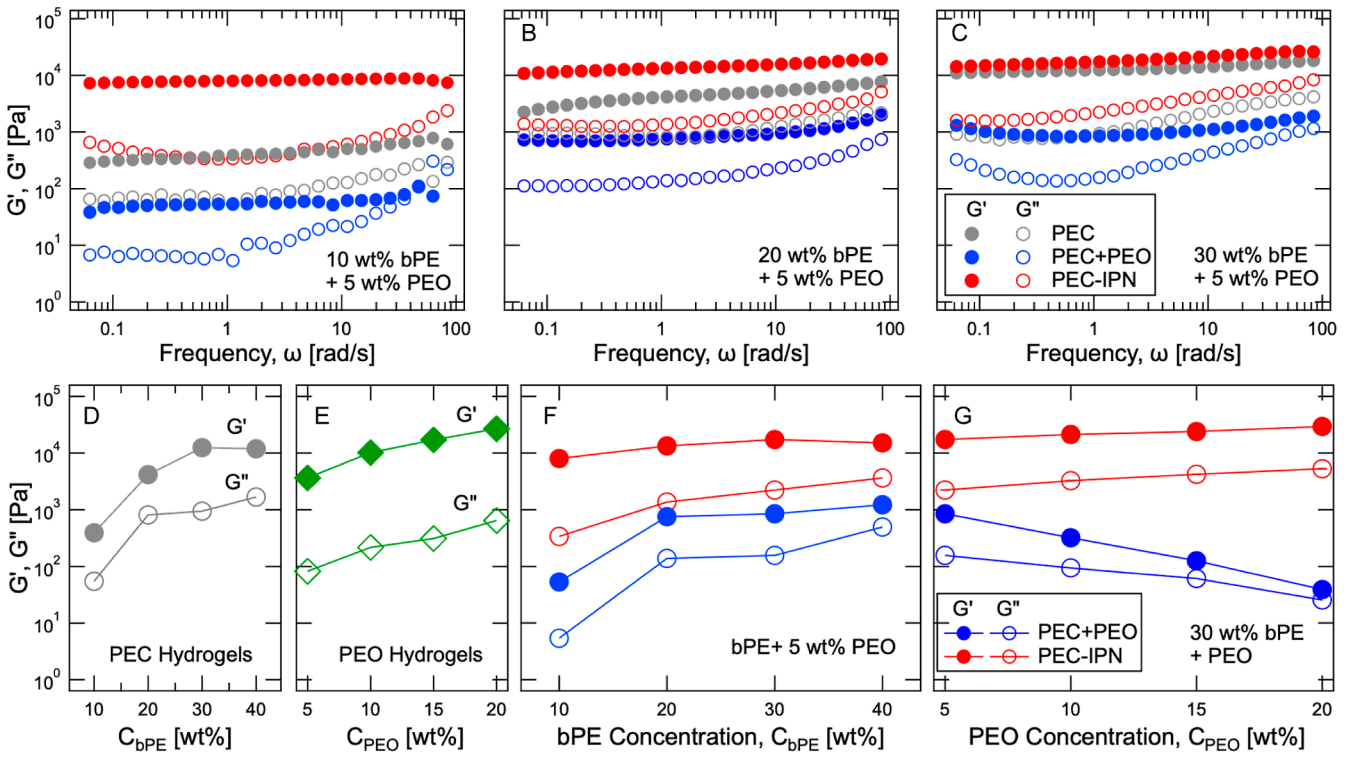

Figure 3. Modulations of shear strength of PEC + PEO and PEC−IPN hydrogels. (A−C) Storage (G') and loss (G'') moduli as a function of frequency (ω), measured by imposing oscillatory strain (strain amplitude γ = 0.3%) on PEC hydrogels (grey), PEC + PEO hydrogels (blue), and PEC−IPN hydrogels (red) with varying C_{bPE} and a constant C_{PEO}. (D−G) G' and G'' (at ω = 1.12 rad/s and γ = 0.3%) for PEC hydrogels with increasing C_{bPE} (D), PEO hydrogels with increasing C_{PEO} (E); and PEC + PEO hydrogels (blue) and PEC−IPN hydrogels (red) with increasing C_{bPE} and constant C_{PEO} = 5 wt % (F) and with increasing C_{PEO} and constant C_{bPE} = 30 wt % (G).

(see also Figure S3A,B). Correspondingly, both R_{PEC} and d_{PEC} for PEC hydrogels (grey symbols), PEC + PEO hydrogels (blue symbols), and PEC−IPN hydrogels (red symbols) evolved near identically with increasing C_{bPE} (Figure 2C).

Tuning the PEO content in the PEC + PEO or the PEC−IPN hydrogels enabled the modulation of the PEC network nanostructure. Morphological transition and ordering of the PEC domains, signified by the appearance of sharp Bragg reflection peaks in the SAXS spectra, shown in Figure 2B, accompanied by a subtle decrease of d_{PEC} (Figure 2D), were observed with increasing C_{PEO} in both PEC + PEO and PEC−IPN hydrogels comprising C_{bPE} = 30 wt %. The relative positions of the primary (q_1), secondary (q_2), and tertiary (q_3) Bragg peaks as q_1:q_2:q_3 ≅ 1:2:3 denote the presence of parallelly stacked lamellar PEC domains in the PEC network with $C_{PEO} \geq$ 15 wt %.

Such morphological and ordering transitions as well as the reduction in domain spacing have been previously observed in PEC hydrogels with increasing bPE concentration[1,4,5,37] and have been hypothesized to arise from the compression of the neutral middle blocks beyond their equilibrium conformations.[5] Here, we expect macromolecular crowding by the 4-arm PEO chains or the covalent network to result in compression and loss of conformational entropy of the PEO midblocks, which in turn induces morphological and ordering transitions in PEC domains. It should be noted that the SAXS spectra shown here are representative of the nearly identical spectra obtained from multiple spots in each of the hydrogel samples, denoting the spatial homogeneity of the hydrogels. Moreover, we note that the PEC domains contain substantial amounts of water,[8,37] and hence, morphological transitions in PEC networks can be induced even in assemblies comprising asymmetric bPE, as opposed to amphiphilic block copolymer assemblies, where lamellar morphologies are expected in polymers with symmetric blocks.

PEC networks comprising weaker ammonium groups instead of strong guanidinium groups in the block polycations exhibit similar behaviors. Guanidinium groups have a higher degree of protonation due to their high pK_a value (~13.6) compared to the ammonium groups (pK_a ~ 9.25), owing to a combination of proton delocalization assisted by resonance stabilization and two binding sites on adjacent nitrogen atoms. The stability of the ionized state of the ionizable groups contributes to the strength of the electrostatic interaction between the oppositely charged blocks and the network properties. Thus, weaker electrostatic interactions between ammonium and sulfonate groups resulted in larger PEC domains and faster equilibration of the PEC network. The resulting PEC hydrogels contained ordered PEC domains at $C_{bPE} \geq$ 30 wt %. The addition of 5 wt % PEO did not disrupt either the disordered or the ordered PEC networks (Figures S5A and S6). Both disordered and ordered PEC networks, although, required smaller C_{PEO} to undergo ordering and morphological transition in PEC + PEO and PEC−IPN hydrogels (Figure S5B). The trends in d_{PEC} and R_{PEC} with varying C_{bPE} and C_{PEO} (Figure S5C,D) remained consistent with the trends shown in Figure 2.

3.3. Modulation of Shear Properties of PEC Hydrogels by Polymer Diluents and Interpenetrating Covalent Networks. PEC hydrogels exhibited frequency-independent storage and loss moduli (G' and G'', respectively) with $G' > G''$, for $C_{bPE} \geq$ 10 wt %, indicating solid-like gels

https://doi.org/10.1021/acs.macromol.2c00590
Macromolecules 2022, 55, 4481−4491

with an absence of terminal relaxation within the time of experiments (grey symbols in Figure 3A−C).[4,5] With increasing C_{bPE}, G' and G'' both increased before G' plateauing around 10 kPa, which is typical for PEC hydrogels (Figure 3D).[4,5] Inclusion of PEO chains in the PEC hydrogels led to a decrease of both G' and G'' while conserving their frequency-independent behavior (blue symbols in Figure 3A−C). Subsequent crosslinking of the PEO chains led to a marked increase in the shear moduli of the resulting PEC−IPN hydrogels, even higher than the corresponding moduli for PEC hydrogels (red symbols in Figure 3A−C).

Figure 3F summarizes the evolution of the shear response of PEC−IPN hydrogels with increasing C_{bPE} for a constant C_{PEO}. The influence of the covalent network on the shear moduli of PEC−IPN hydrogels was more pronounced when the covalent network served as the primary load-bearing network. When the shear moduli of PEC hydrogels with $C_{bPE} \leq 20$ wt % (Figure 3D) were smaller than of the 5 wt % covalent hydrogels (Figures 3E and S7), the corresponding PEC−IPN hydrogels exhibited more than two-fold improvement in both G' and G'' as compared to the PEC hydrogels (Figure 3D,F, see also Figure 3A,B). In contrast, only modest enhancements in moduli were achieved in PEC−IPN hydrogels with $C_{bPE} > 20$ wt %. At high bPE concentrations, loop formation as well as hindrance of the photocrosslinking of the PEO chains by the PEC network can reduce the shear moduli contributions from the PEO network to the IPN hydrogels. Importantly, because the moduli of the covalent PEO network are directly proportional to the C_{PEO} (Figure 3E), PEO content in the PEC−IPN hydrogels can be harnessed as a facile route to tune their moduli. As an illustration, steady improvements in G' and G'' of PEC−IPN hydrogels with $C_{bPE} = 30$ wt % were observed upon increasing C_{PEO} (Figure 3C,D,G see also Figure S8).

These moduli enhancements serve as an indicator of the interpenetrating nature of the PEC and the covalent networks and their synergistic contribution to the shear strength of the resulting hybrid hydrogel. The interlacing of the two networks is hypothesized to introduce further entanglements between them, in effect acting as additional crosslinks, leading to higher moduli of the IPN hydrogels as compared to hydrogels comprising either of the components. The synergy between the two networks is further illustrated through a comparison of the moduli of the PEC−IPN hydrogels with the sum of the moduli of the constituent networks (Figure S9). Both G' and G'' for the PEC−IPN hydrogels were found to be larger than the linear combination of the respective moduli of the constituent networks in most cases, except for the PEC−IPN hydrogels with high C_{bPE} (= 30 wt %) and C_{PEO} (>15 wt %). In these hydrogels, the high polymer concentration can be expected to hinder the crosslinking of the PEO network, resulting in loop formation or unreacted PEO ends, or both. Overall, PEC−IPN hydrogels exhibit superior shear strength which either PEC hydrogels or covalent hydrogels cannot achieve either individually or, in most cases, in a linear combination with each other.

In contrast, PEC + PEO hydrogels exhibit a marked decrease in shear strength as compared to the PEC hydrogels (blue symbols in Figure 3A−C,F). Increasing PEO content in PEC + PEO hydrogels led to the continuing reduction of G' and G'' (Figure 3G). We hypothesize that this reduction can be attributed to a reconfiguration of the PEC network by the 4-arm PEO chains. Previously, it has been shown that self-assembly of symmetric, oppositely charged *ABA* triblock polyelectrolytes results in networks with a higher-than-expected fraction of *B* blocks forming bridges instead of loops, manifesting as gel formation at surprisingly low polymer concentrations.[3] Here, we argue that the inclusion of 4-arm PEO chains induces macromolecular crowding, hindering bridge formation and promoting loop formation, reducing the network connectivity and reducing its shear moduli. Furthermore, the injectability of the PEC network containing precursor solutions can also be tuned precisely. The PEC + PEO hydrogels exhibit strong shear thinning characteristics (Figure S10A−D) and the microstructure of the PEC networks recovers quickly after strong shearing (Figure S10E),[72] resulting in facile injection and swift recovery of the hydrogel elasticity post injection (Figure 1B, row 3).

We note that the PEC + PEO and the PEC−IPN hydrogels are both expected to be spatially uniform, and therefore, spatial inhomogeneities and phase separation are not expected to play a role in contributing to the observed decay of the PEC + PEO hydrogel moduli. The mixing protocols, comprising mixing of the 4-arm PEO and the block polyanions before the addition of the block polycations, ensured uniform mixing of the polymers. Additionally, SAXS spectra collected from various locations in the hydrogel samples were identical, pointing toward a spatially homogenous distribution of the PEC domains. We also note that the drop in the moduli with increasing ω in the low ω ($\lesssim$0.5 rad/s) range in frequency sweeps for PEC + PEO hydrogels in Figures 3C and S8D indicates that the hydrogel was equilibrating while the initial low ω moduli measurements were made. We attribute this trend to the specific measurement protocol we followed where the shearing frequency of the sample jumped from ω = 1 Hz to ω = 0.01 Hz nearly instantaneously upon transition from the preshearing step to the frequency sweep measurements. For the other PEC + PEO, PEC, and PEC−IPN hydrogels, the moduli are ω independent and, therefore, did not show any effect of this change in the shearing frequency. However, for the PEC + PEO hydrogels with $C_{bPE} \geq 30$ and 5 wt % PEO, the moduli are frequency dependent, and the recovery and equilibration of the samples are evident in the first few points in the frequency sweep.

Similar trends were observed in PEC, PEC + PEO, and PEC−IPN hydrogels comprising ammonium and sulfonated bPEs (Figure S11). These PEC hydrogels exhibited G' and G'' that were lower than the corresponding guanidinilated bPE-containing PEC hydrogels, and both moduli exhibited a maximum with increasing C_{bPE} owing to the morphological transitions of the PEC domains.[5] G' and G'' of these PEC hydrogels were lower even than that of 5 wt % 4-arm PEO hydrogels across C_{bPE} varying from 10 to 40 wt %. Thus, distinct improvements in the moduli were achieved in PEC−IPN hydrogels compared to the PEC hydrogels upon the introduction of 5 wt % PEO (Figure S11H). Moreover, similar to variations depicted in Figure 3G, PEC−IPN and PEC + PEO hydrogel moduli varied continually with increasing C_{PEO} (Figure S11I).

3.4. Imparting Tensile Strength to PEC Hydrogels by Interpenetration with Covalent Networks. Combining PEC networks with covalent networks also rendered tensile strength and extensibility to PEC−IPN hydrogels, characteristics that are inaccessible to PEC hydrogels, as illustrated in the representative stress−strain curves obtained from uniaxial tensile testing in Figure 4. The physically crosslinked PEC hydrogels do not possess tensile strength as the block polyelectrolyte chains can rearrange readily when subjected

https://doi.org/10.1021/acs.macromol.2c00590
Macromolecules 2022, 55, 4481−4491

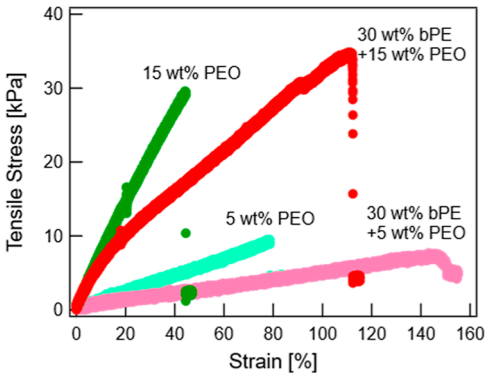

Figure 4. Imparting tensile strength to PEC network *via* PEC−IPN hydrogels. Representative stress curves as a function of strain for PEO and PEC−IPN hydrogels with C_{bPE} = 30 wt % and C_{PEO} = 5 or 15 wt %.

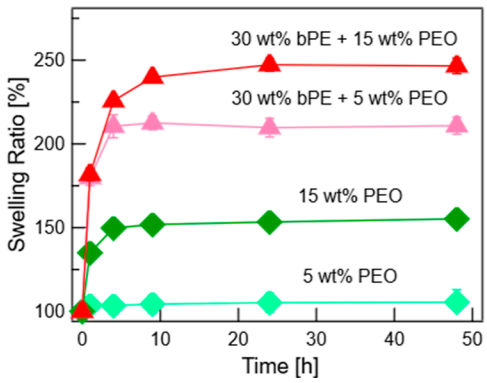

Figure 5. Controlling the swelling behavior of PEC network by interpenetration with covalent networks. The swelling of PEO and PEC−IPN hydrogels with C_{bPE} = 30 wt % and C_{PEO} = 5 or 15 wt %, as denoted by their weight gain over time.

to tensile strain. In contrast, covalently crosslinked PEO hydrogels exhibit elasticity emerging from the finite extensibility of the polymer chains between the crosslinks. In PEC−IPN hydrogels, the covalent network is hypothesized to provide the tension points while the self-assembled domains that comprise the PEC network serve as energy-dissipating physical multi-linkages. The ultimate strength of the PEC−IPN hydrogels (C_{PEO} = 5 or 15 wt % + C_{bPE} = 30 wt %) was found to remain comparable to that of the corresponding covalent hydrogels, with minor loss of strength (Figure S12A). At the same time, as compared to corresponding PEO hydrogels, PEC−IPN hydrogels exhibit improvements in both extensibility and toughness (Figure S12B,C).

These improvements can be attributed to the reconfigurable nature of the PEC network that enables network restructuring and promotes stress dissipation. Network restructuring is further evident in the distinct two-step stress growth during uniaxial stretching of the PEC−IPN hydrogels (Figures 4, see also S13). At the same time, the formation of the covalent network may be hindered partially by the PEC network, resulting in lower ultimate strength but contributing to higher extensibility. Similar enhancements in tensile performance were also noted upon replacing the guanidinium moieties with ammonium moieties in the bPEs comprising the PEC−IPN hydrogels (Figures S14 and S15).

3.5. Modulating the Response of PEC Hydrogels to Aqueous or Saline Environments. Figure 5 presents representative data highlighting the swelling characteristics of the PEC−IPN hydrogels. PEC−IPN hydrogels swelled more than their corresponding PEO hydrogels yet reached equilibrium within a few hours. Swelling in all hydrogels was found to plateau within 24 h. The larger swelling of the PEC−IPN hydrogels could be attributed to the hydrophilic bPEs absorbing larger amounts of water, providing an excess osmotic pressure to further expand the interpenetrating polymer networks and partially hindering the formation of the covalent network in the PEC−IPN hydrogels enabling its larger expansion and resulting in loss of uncrosslinked chains into the surrounding solution. At the same time, some of the bPE chains can also be expected to leave the PEC network and dissolve in the surrounding solution, although their fraction is expected to be very small owing to the extremely small fraction of uncomplexed bPE chains in the PEC networks.[3] The swelling of PEC−IPN hydrogels could be tuned by varying C_{PEO}; the swelling ratio of PEC−IPN hydrogels increased by 18% upon increasing C_{PEO} from 5 to 15 wt %. This is commensurate with the larger swelling of the 15 wt % PEO hydrogels as compared to the 5 wt % PEO hydrogels (Figure 5). Again, these are distinct improvements over the indefinite swelling of PEC hydrogels, ascribable to their physically crosslinked structure.

PEC−IPN hydrogels also retained their mechanical strength upon exposure to salt. The introduction of salt resulted in a progressive breakdown of the PEC network, evident from the broadening peaks in the SAXS spectra obtained from PEC−IPN hydrogels (C_{bPE} = 30 wt %, C_{PEO} = 5 wt %) with increasing salt concentrations (Figure 6A,C, see also Figure S16A,D). The influence of salt on the network microstructure was more evident in PEC networks containing ammonium functionalized bPEs (Figure 6C) as compared to guanidinilated bPEs (Figure 6A). Correspondingly, shear moduli of PEC hydrogels with guanidinium moieties decreased by ∼2 orders of magnitude upon increasing C_{salt} up to 600 mM (grey symbols in Figure 6B, see also Figure S16B,C) while the moduli of the PEC hydrogels with ammonium moieties decreased precipitously with increasing C_{salt}. In contrast, the corresponding PEC−IPN hydrogels exhibited far superior shear strength even when the PEC network was disrupted, ascribable to the presence of the covalent network that sustains the shear response of the hydrogels in salty environments (red symbols in Figure 6B,D, see also Figure S16E,F). Thus, the PEC−IPN hydrogels present a possibility of hydrogel design wherein ionic strength or pH can be varied to induce changes in network microstructure while retaining controlled moduli and swelling responses.

4. CONCLUSIONS AND IMPLICATIONS IN BIOMATERIALS DEVELOPMENT

In summary, we have demonstrated, for the first time, a facile approach for creating PEC−IPN hydrogels composed of interpenetrating PEC networks (composed of oppositely charged block polyelectrolytes) and covalent networks (composed of photocrosslinked 4-arm PEO chains). PEC−IPN hydrogels are shown to possess superior shear and tensile properties which cannot be achieved by either of the individual networks. Moreover, the PEC−IPN hydrogels exhibit enhanced mechanical stability in salt environments and a tunable swelling response.

https://doi.org/10.1021/acs.macromol.2c00590
Macromolecules 2022, 55, 4481−4491

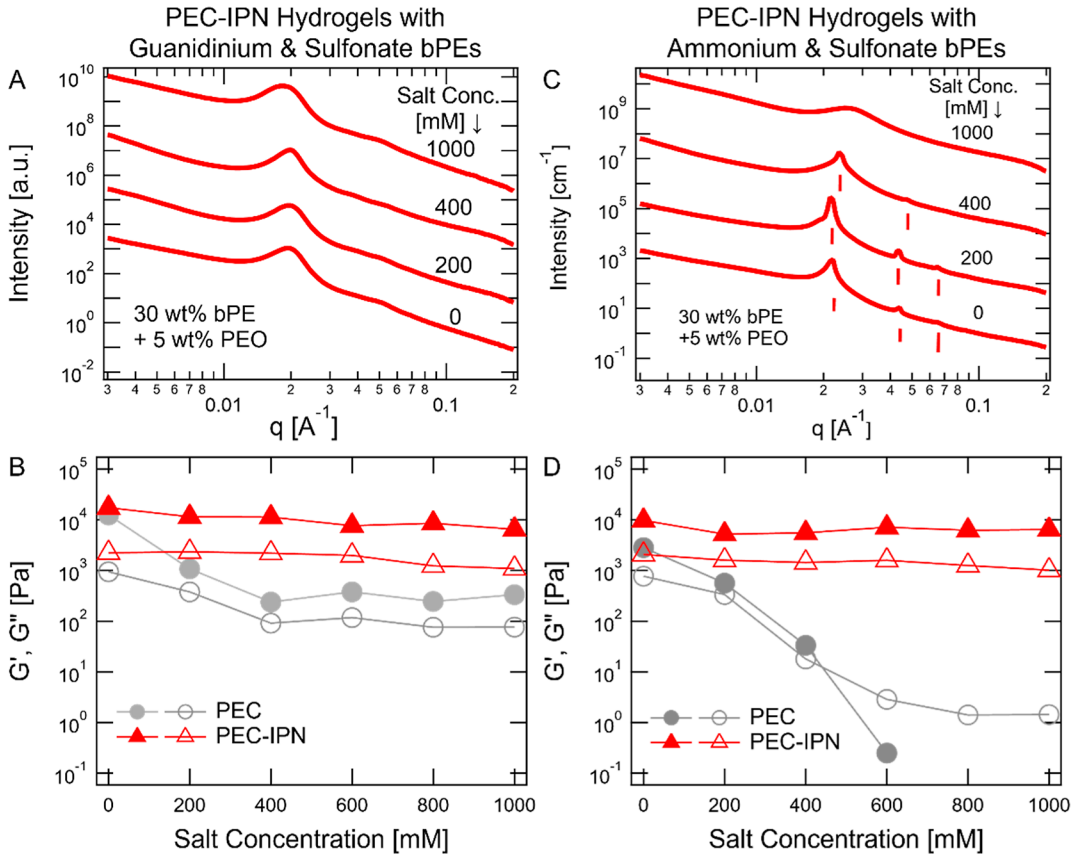

Figure 6. Evolution of microstructure and shear strength of PEC−IPN hydrogels in saline environments. (A) One-dimensional SAXS intensities $I(q)$ *vs* wave vector q and (B) shear moduli (G' and G''), measured at ω = 1.12 rad/s and γ = 0.3%, as a function of salt concentration C_{salt} for PEC−IPN hydrogels (C_{bPE} = 30 wt % + C_{PEO} = 5 wt %) composed of bPEs functionalized with guanidinium and sulfonate moieties. In (B), corresponding G' and G'' data are also shown for PEC hydrogels (C_{bPE} = 30 wt %). (C,D) show data corresponding to (A,B), respectively for PEC−IPN hydrogels (C_{bPE} = 30 wt % + C_{PEO} = 5 wt %) and PEC hydrogels (C_{bPE} = 30 wt %) composed of bPEs functionalized with ammonium and sulfonate moieties. In (A,C), the $I(q)$ spectra were shifted vertically for clarity. See Supporting Information Table S2 for peak assignments in (C).

The PEO chains and networks, at sufficiently high loadings, induce morphological and ordering transitions in the PEC domains, providing a handle to tune the PEC domain morphologies and arrangements. At the same time, the interpenetration of the PEC network with the covalent network enables an independent modulation of the shear properties of the PEC network. PEC−IPN hydrogels with interpenetrating covalent and PEC networks featured G' > 10 kPa, a regime rarely accessible by PEC hydrogels but is important for the design of strong hydrogels and adhesives.

These improved features of the PEC−IPN hydrogels, as compared to PEC hydrogels, are highly desirable in numerous biomedical applications. For instance, the PEC−IPN hydrogels demonstrated here can serve as a model platform to establish routes for the use of materials based on block polyelectrolyte self-assembly in biomedical applications as adhesives and scaffolding wherein control over the gel microstructure (and drug loading capacity), shear and tensile strength, and extensibility are sought.

In parallel, the platform can act as a facile method to address current challenges associated with the use of photocrosslinkable polymers in advanced materials and biomedicine. PEC hydrogels can serve as a protective scaffolding, preventing uncontrolled dilution of the precursor solution and avoiding material loss and functional deactivation in wet environments. Moreover, the crosslinked gels can achieve higher moduli owing to the interpenetrating PEC network. Thus, the combination of existing photocrosslinkable polymers and PEC hydrogels represents a promising one-pot solution that could be employed directly on the application site without additional processing steps. These improvements can prove very beneficial for various applications where photocrosslinked hydrogels are employed, especially applications where *in situ* crosslinking of the precursor polymers is sought.[73,74] For instance, light-based biofabrication processes, such as extrusion-based 3D printing, that face issues of low viscosity and weak structural integrity of the hydrogel precursor solution prior to photocrosslinking can benefit from the inclusion of PEC networks into the 3-D printing inks. Such a combination can achieve initial shear strength, minimize loss of precursor from secondary flows, and promote interlayer bonding, paving the way for high-resolution printing.[74] Similarly, drug-loaded hydrogel patches or adhesive tissue sealants that rely on chemical crosslinking of precursors *in situ* can also benefit from the introduction of PEC networks in the precursor solution. The injectable precursor solutions in these applications typically possess a low viscosity and tend to perfuse from the site of injection into the surrounding tissue, leading to premature release of their drug cargo or weak and ineffective adhesion, respectively.[73] Incorporation of PEC networks can reinforce the mechanical properties of the injected hydrogel

https://doi.org/10.1021/acs.macromol.2c00590
Macromolecules 2022, 55, 4481−4491

precursors and, thus, mitigate the loss of precursor molecules and reduce their dosage.

■ ASSOCIATED CONTENT

Supporting Information

The Supporting Information is available free of charge at https://pubs.acs.org/doi/10.1021/acs.macromol.2c00590.

^{1}H NMR spectra of $PAGE_{98}$−PEO_{455}−$PAGE_{98}$; amplitude sweeps showing the shear moduli (G′ and G″) as a function of strain for PEO, PEC, PEC+PEO, and PEC-IPN hydrogels; SAXS scattering spectra and PEC domain attributes of PEC, PEC+PEO, and PEC-IPN hydrogels; fitting curves to determine PEC domain core radius of PEC hydrogels; shear strength of PEC, PEC +PEO, and PEC-IPN hydrogels; synergistic shear response of guanidinium & sulfonate PEC-IPN hydrogels; complex viscosity and cyclic strain performance of PEC and PEC+PEO hydrogels; modulations of shear strengths of PEC, PEO, PEC+PEO, and PEC-IPN hydrogels; stress vs. strain curves and tensile characterization of PEO and PEC-IPN hydrogels; evolution of microstructure and shear strength of PEC-IPN hydrogels; and Bragg peak locations and microstructure information (PDF)

Injection, settling, and insolubility upon shaking of PEC hydrogels with C_{bPE} = 10 wt% (MOV)

Injection, settling, and insolubility upon shaking of PEC +PEO hydrogels with C_{bPE} = 10 wt% and C_{PEO} = 5 wt% (MOV)

Injection, settling, and solubility upon shaking of PEO precursor polymers with C_{PEO} = 5 wt% (MOV)

■ AUTHOR INFORMATION

Corresponding Author

Samanvaya Srivastava − *Department of Chemical and Biomolecular Engineering, California NanoSystems Institute, Center for Biological Physics, and Institute for Carbon Management, University of California, Los Angeles, Los Angeles, California 90095, United States;* orcid.org/0000-0002-3519-7224; Email: samsri@ucla.edu

Authors

Defu Li − *Department of Chemical and Biomolecular Engineering, University of California, Los Angeles, Los Angeles, California 90095, United States*

Tobias Göckler − *Department of Chemical and Biomolecular Engineering, University of California, Los Angeles, Los Angeles, California 90095, United States; Institute of Functional Interfaces, Karlsruhe Institute of Technology, Eggenstein-Leopoldshafen 76344, Germany*

Ute Schepers − *Institute of Functional Interfaces, Karlsruhe Institute of Technology, Eggenstein-Leopoldshafen 76344, Germany; Institute of Organic Chemistry, Karlsruhe Institute of Technology, Karlsruhe 76131, Germany*

Complete contact information is available at: https://pubs.acs.org/10.1021/acs.macromol.2c00590

Funding

This research was supported by the National Science Foundation under grant no. DMR-2048285. Support for T. G. and U. S. was provided by the Deutsche Forschungsgemeinschaft (DFG, German Research Foundation) under Germany's Excellence Strategy *via* the Excellence Cluster 3D Matter Made to Order (EXC-2082/1−390761711) and by the Bundesministerium für Bildung und Forschung (BMBF) by the KMU-NetC 3D-Bio-Net (FKZ 03VNE1034D). T.G. acknowledges financial support from the Karlsruhe House of Young Scientists (KHYS) and is funded by a Kekulé Fellowship of the Chemical Industry Fund.

Notes

The authors declare no competing financial interest.

■ ACKNOWLEDGMENTS

This research uses the facility of the Advanced Photon Sources, a U.S. Department of Energy (DOE) Office of Science User Facility operated for the DOE Office of Science by Argonne National Laboratory under Contract No. DE-AC02-06CH11357. D.L. acknowledges the access to the Instron 5542 tester by Prof. Nasim Annabi and her research group. S.S. acknowledges helpful discussion with Prof. Vivek Sharma.

■ REFERENCES

(1) Hunt, J. N.; Feldman, K. E.; Lynd, N. A.; Deek, J.; Campos, L. M.; Spruell, J. M.; Hernandez, B. M.; Kramer, E. J.; Hawker, C. J. Tunable, High Modulus Hydrogels Driven by Ionic Coacervation. *Adv. Mater.* **2011**, *23*, 2327−2331.

(2) Lemmers, M.; Sprakel, J.; Voets, I. K.; van der Gucht, J.; Cohen Stuart, M. A. Multiresponsive Reversible Gels Based on Charge-Driven Assembly. *Angew. Chem.* **2010**, *122*, 720−723.

(3) Srivastava, S.; Andreev, M.; Levi, A. E.; Goldfeld, D. J.; Mao, J.; Heller, W. T.; Prabhu, V. M.; de Pablo, J. J.; Tirrell, M. V. Gel Phase Formation in Dilute Triblock Copolyelectrolyte Complexes. *Nat. Commun.* **2017**, *8*, 14131.

(4) Krogstad, D. V.; Lynd, N. A.; Choi, S.-H.; Spruell, J. M.; Hawker, C. J.; Kramer, E. J.; Tirrell, M. V. Effects of Polymer and Salt Concentration on the Structure and Properties of Triblock Copolymer Coacervate Hydrogels. *Macromolecules* **2013**, *46*, 1512−1518.

(5) Srivastava, S.; Levi, A. E.; Goldfeld, D. J.; Tirrell, M. V. Structure, Morphology, and Rheology of Polyelectrolyte Complex Hydrogels Formed by Self-Assembly of Oppositely Charged Triblock Polyelectrolytes. *Macromolecules* **2020**, *53*, 5763−5774.

(6) Lemmers, M.; Spruijt, E.; Beun, L.; Fokkink, R.; Leermakers, F.; Portale, G.; Cohen Stuart, M. A.; van der Gucht, J. The Influence of Charge Ratio on Transient Networks of Polyelectrolyte Complex Micelles. *Soft Matter* **2012**, *8*, 104−117.

(7) Lemmers, M.; Spruijt, E.; Akerboom, S.; Voets, I. K.; van Aelst, A. C.; Cohen Stuart, M. A.; van der Gucht, J. Physical Gels Based on Charge-Driven Bridging of Nanoparticles by Triblock Copolymers. *Langmuir* **2012**, *28*, 12311−12318.

(8) Krogstad, D. V.; Choi, S.-H.; Lynd, N. A.; Audus, D. J.; Perry, S. L.; Gopez, J. D.; Hawker, C. J.; Kramer, E. J.; Tirrell, M. V. Small Angle Neutron Scattering Study of Complex Coacervate Micelles and Hydrogels Formed from Ionic Diblock and Triblock Copolymers. *J. Phys. Chem. B* **2014**, *118*, 13011−13018.

(9) Krogstad, D. V.; Lynd, N. A.; Miyajima, D.; Gopez, J.; Hawker, C. J.; Kramer, E. J.; Tirrell, M. V. Structural Evolution of Polyelectrolyte Complex Core Micelles and Ordered-Phase Bulk Materials. *Macromolecules* **2014**, *47*, 8026−8032.

(10) Cui, H.; Zhuang, X.; He, C.; Wei, Y.; Chen, X. High Performance and Reversible Ionic Polypeptide Hydrogel Based on Charge-Driven Assembly for Biomedical Applications. *Acta Biomater.* **2015**, *11*, 183−190.

(11) Papadakis, C.; Tsitsilianis, C. Responsive Hydrogels from Associative Block Copolymers: Physical Gelling Through Polyion Complexation. *Gels* **2017**, *3*, 3.

(12) Kim, J.-M.; Heo, T.-Y.; Choi, S.-H. Structure and Relaxation Dynamics for Complex Coacervate Hydrogels Formed by ABA Triblock Copolymers. *Macromolecules* **2020**, *53*, 9234−9243.

(13) Seliktar, D. Designing Cell-Compatible Hydrogels for Biomedical Applications. *Science* **2012**, *336*, 1124−1128.
(14) Zhang, Y. S.; Khademhosseini, A. Advances in Engineering Hydrogels. *Science* **2017**, *356*, No. eaaf3627.
(15) Lee, K. Y.; Mooney, D. J. Hydrogels for Tissue Engineering. *Chem. Rev.* **2001**, *101*, 1869−1880.
(16) Nguyen, K. T.; West, J. L. Photopolymerizable Hydrogels for Tissue Engineering Applications. *Biomaterials* **2002**, *23*, 4307−4314.
(17) Khademhosseini, A.; Langer, R. Microengineered Hydrogels for Tissue Engineering. *Biomaterials* **2007**, *28*, 5087−5092.
(18) Wang, H.; Heilshorn, S. C. Adaptable Hydrogel Networks with Reversible Linkages for Tissue Engineering. *Adv. Mater.* **2015**, *27*, 3717−3736.
(19) Mehdizadeh, M.; Yang, J. Design Strategies and Applications of Tissue Bioadhesives. *Macromol. Biosci.* **2013**, *13*, 271−288.
(20) Peak, C. W.; Wilker, J. J.; Schmidt, G. A Review on Tough and Sticky Hydrogels. *Colloid Polym. Sci.* **2013**, *291*, 2031−2047.
(21) Scognamiglio, F.; Travan, A.; Rustighi, I.; Tarchi, P.; Palmisano, S.; Marsich, E.; Borgogna, M.; Donati, I.; de Manzini, N.; Paoletti, S. Adhesive and Sealant Interfaces for General Surgery Applications. *J. Biomed. Mater. Res., Part B* **2016**, *104*, 626−639.
(22) Kord Forooshani, P.; Lee, B. P. Recent Approaches in Designing Bioadhesive Materials Inspired by Mussel Adhesive Protein. *J. Polym. Sci., Part A: Polym. Chem.* **2017**, *55*, 9−33.
(23) Bhagat, V.; Becker, M. L. Degradable Adhesives for Surgery and Tissue Engineering. *Biomacromolecules* **2017**, *18*, 3009−3039.
(24) Li, J.; Celiz, A. D.; Yang, J.; Yang, Q.; Wamala, I.; Whyte, W.; Seo, B. R.; Vasilyev, N. V.; Vlassak, J. J.; Suo, Z.; Mooney, D. J. Tough Adhesives for Diverse Wet Surfaces. *Science* **2017**, *357*, 378−381.
(25) Chen, X.; Yuk, H.; Wu, J.; Nabzdyk, C. S.; Zhao, X. Instant Tough Bioadhesive with Triggerable Benign Detachment. *Proc. Natl. Acad. Sci. U.S.A.* **2020**, *117*, 15497−15503.
(26) Gao, Y.; Han, X.; Chen, J.; Pan, Y.; Yang, M.; Lu, L.; Yang, J.; Suo, Z.; Lu, T. Hydrogel-Mesh Composite for Wound Closure. *Proc. Natl. Acad. Sci. U.S.A.* **2021**, *118*, No. e2103457118.
(27) Hoare, T. R.; Kohane, D. S. Hydrogels in Drug Delivery: Progress and Challenges. *Polymer* **2008**, *49*, 1993−2007.
(28) Kesharwani, P.; Bisht, A.; Alexander, A.; Dave, V.; Sharma, S. Biomedical Applications of Hydrogels in Drug Delivery System: An Update. *J. Drug Deliv. Sci. Technol.* **2021**, *66*, 102914.
(29) Li, J.; Mooney, D. J. Designing Hydrogels for Controlled Drug Delivery. *Nat. Rev. Mater.* **2016**, *1*, 16071.
(30) Dimatteo, R.; Darling, N. J.; Segura, T. In situ Forming Injectable Hydrogels for Drug Delivery and Wound Repair. *Adv. Drug Delivery Rev.* **2018**, *127*, 167−184.
(31) Pakulska, M. M.; Vulic, K.; Tam, R. Y.; Shoichet, M. S. Hybrid Crosslinked Methylcellulose Hydrogel: A Predictable and Tunable Platform for Local Drug Delivery. *Adv. Mater.* **2015**, *27*, 5002−5008.
(32) Yang, C.; Suo, Z. Hydrogel Ionotronics. *Nat. Rev. Mater.* **2018**, *3*, 125−142.
(33) Deng, J.; Yuk, H.; Wu, J.; Varela, C. E.; Chen, X.; Roche, E. T.; Guo, C. F.; Zhao, X. Electrical Bioadhesive Interface for Bioelectronics. *Nat. Mater.* **2020**, *20*, 229−236.
(34) Cao, Y.; Mezzenga, R. Design Principles of Food Gels. *Nat. Food* **2020**, *1*, 106−118.
(35) Li, J.; Jia, X.; Yin, L. Hydrogel: Diversity of Structures and Applications in Food Science. *Food Rev. Int.* **2021**, *37*, 313−372.
(36) Jiang, J.; Chen, E.-Q.; Yang, S. The Effect of Ion Pairs on Coacervate-Driven Self-Assembly of Block Polyelectrolytes. *J. Chem. Phys.* **2021**, *154*, 144903.
(37) Audus, D. J.; Gopez, J. D.; Krogstad, D. V.; Lynd, N. A.; Kramer, E. J.; Hawker, C. J.; Fredrickson, G. H. Phase Behavior of Electrostatically Complexed Polyelectrolyte Gels Using an Embedded Fluctuation Model. *Soft Matter* **2015**, *11*, 1214−1225.
(38) Audus, D. J.; Fredrickson, G. H. Field-Based Simulations of Nanostructured Polyelectrolyte Gels. In *Materials for Energy Infrastructure*; Springer: Singapore, 2016, pp 1−9.
(39) Staňo, R.; Košovan, P.; Tagliabue, A.; Holm, C. Electrostatically Cross-Linked Reversible Gels—Effects of pH and Ionic Strength. *Macromolecules* **2021**, *54*, 4769−4781.
(40) Sun, T. L.; Kurokawa, T.; Kuroda, S.; Ihsan, A. B.; Akasaki, T.; Sato, K.; Haque, M. A.; Nakajima, T.; Gong, J. P. Physical Hydrogels Composed of Polyampholytes Demonstrate High Toughness and Viscoelasticity. *Nat. Mater.* **2013**, *12*, 932.
(41) Shi, R.; Sun, T. L.; Luo, F.; Nakajima, T.; Kurokawa, T.; Bin, Y. Z.; Rubinstein, M.; Gong, J. P. Elastic−Plastic Transformation of Polyelectrolyte Complex Hydrogels from Chitosan and Sodium Hyaluronate. *Macromolecules* **2018**, *51*, 8887−8898.
(42) Sun, T. L.; Cui, K.; Gong, J. P. Tough, Self-Recovery and Self-Healing Polyampholyte Hydrogels. *Polym. Sci., Ser. C* **2017**, *59*, 11−17.
(43) Fan, H.; Wang, J.; Gong, J. P. Barnacle Cement Proteins-Inspired Tough Hydrogels with Robust, Long-Lasting, and Repeatable Underwater Adhesion. *Adv. Funct. Mater.* **2020**, *31*, 2009334.
(44) Li, S.; Pan, H.; Wang, Y.; Sun, J. Polyelectrolyte Complex-Based Self-Healing, Fatigue-Resistant and Anti-Freezing Hydrogels as Highly Sensitive Ionic Skins. *J. Mater. Chem. A* **2020**, *8*, 3667−3675.
(45) Luo, F.; Sun, T. L.; Nakajima, T.; Kurokawa, T.; Zhao, Y.; Sato, K.; Ihsan, A. B.; Li, X.; Guo, H.; Gong, J. P. Oppositely Charged Polyelectrolytes Form Tough, Self-Healing, and Rebuildable Hydrogels. *Adv. Mater.* **2015**, *27*, 2722−2727.
(46) Li, G.; Zhang, G.; Sun, R.; Wong, C.-P. Dually pH-Responsive Polyelectrolyte Complex Hydrogel Composed of Polyacrylic Acid and Poly (2-(Dimthylamino) Ethyl Methacrylate). *Polymer* **2016**, *107*, 332−340.
(47) Liu, Q.; Dong, Z.; Ding, Z.; Hu, Z.; Yu, D.; Hu, Y.; Abidi, N.; Li, W. Electroresponsive Homogeneous Polyelectrolyte Complex Hydrogels from Naturally Derived Polysaccharides. *ACS Sustainable Chem. Eng.* **2018**, *6*, 7052−7063.
(48) Lemmers, M.; Voets, I. K.; Cohen Stuart, M. A.; van der Gucht, J. Transient Network Topology of Interconnected Polyelectrolyte Complex Micelles. *Soft Matter* **2011**, *7*, 1378−1389.
(49) Lee, A. L. Z.; Voo, Z. X.; Chin, W.; Ono, R. J.; Yang, C.; Gao, S.; Hedrick, J. L.; Yang, Y. Y. Injectable Coacervate Hydrogel for Delivery of Anticancer Drug-Loaded Nanoparticles in vivo. *ACS Appl. Mater. Interfaces* **2018**, *10*, 13274−13282.
(50) Gao, S.; Holkar, A.; Srivastava, S. Protein-Polyelectrolyte Complexes and Micellar Assemblies. *Polymers* **2019**, *11*, 1097.
(51) Magana, J. R.; Sproncken, C. C. M.; Voets, I. K. On Complex Coacervate Core Micelles: Structure-Function Perspectives. *Polymers* **2020**, *12*, 1953.
(52) Chen, F.; Stenzel, M. H. Polyion Complex Micelles for Protein Delivery. *Aust. J. Chem.* **2018**, *71*, 768−780.
(53) Horn, J.; Kapelner, R.; Obermeyer, A. Macro-and Microphase Separated Protein-Polyelectrolyte Complexes: Design Parameters and Current Progress. *Polymers* **2019**, *11*, 578.
(54) Shah, S.; Leon, L. Structural Dynamics, Phase behavior, and Applications of Polyelectrolyte Complex Micelles. *Curr. Opin. Colloid Interface Sci.* **2021**, *53*, 101424.
(55) Discher, D. E.; Mooney, D. J.; Zandstra, P. W. Growth Factors, Matrices, and Forces Combine and Control Stem Cells. *Science* **2009**, *324*, 1673−1677.
(56) Engler, A. J.; Sen, S.; Sweeney, H. L.; Discher, D. E. Matrix Elasticity Directs Stem Cell Lineage Specification. *Cell* **2006**, *126*, 677−689.
(57) Discher, D. E.; Janmey, P.; Wang, Y.-l. Tissue Cells Feel and Respond to the Stiffness of Their Substrate. *Science* **2005**, *310*, 1139−1143.
(58) Kamata, H.; Li, X.; Chung, U.-i.; Sakai, T. Design of Hydrogels for Biomedical Applications. *Adv. Healthcare Mater.* **2015**, *4*, 2360−2374.
(59) Yang, H.; Ghiassinejad, S.; van Ruymbeke, E.; Fustin, C.-A. Tunable Interpenetrating Polymer Network Hydrogels Based on Dynamic Covalent Bonds and Metal−Ligand Bonds. *Macromolecules* **2020**, *53*, 6956−6967.

https://doi.org/10.1021/acs.macromol.2c00590
Macromolecules 2022, 55, 4481−4491

(60) Dhand, A. P.; Galarraga, J. H.; Burdick, J. A. Enhancing Biopolymer Hydrogel Functionality through Interpenetrating Networks. *Trends Biotechnol.* **2021**, *39*, 519−538.
(61) Waters, D. J.; Engberg, K.; Parke-Houben, R.; Ta, C. N.; Jackson, A. J.; Toney, M. F.; Frank, C. W. Structure and Mechanism of Strength Enhancement in Interpenetrating Polymer Network Hydrogels. *Macromolecules* **2011**, *44*, 5776−5787.
(62) Dragan, E. S. Design and Applications of Interpenetrating Polymer Network Hydrogels. A Review. *Chem. Eng. J.* **2014**, *243*, 572−590.
(63) Myung, D.; Waters, D.; Wiseman, M.; Duhamel, P.-E.; Noolandi, J.; Ta, C. N.; Frank, C. W. Progress in the Development of Interpenetrating Polymer Network Hydrogels. *Polym. Adv. Technol.* **2008**, *19*, 647−657.
(64) Silverstein, M. S. Interpenetrating Polymer Networks: So Happy Together? *Polymer* **2020**, *207*, 122929.
(65) Ilavsky, J.; Jemian, P. R. Irena: Tool Suite for Modeling and Analysis of Small-Angle Scattering. *J. Appl. Crystallogr.* **2009**, *42*, 347−353.
(66) Wu, H.; Ting, J. M.; Yu, B.; Jackson, N. E.; Meng, S.; de Pablo, J. J.; Tirrell, M. V. Spatiotemporal Formation and Growth Kinetics of Polyelectrolyte Complex Micelles with Millisecond Resolution. *ACS Macro Lett.* **2020**, *9*, 1674−1680.
(67) Takahashi, R.; Narayanan, T.; Yusa, S.-i.; Sato, T. Formation Kinetics of Polymer Vesicles from Spherical and Cylindrical Micelles Bearing the Polyelectrolyte Complex Core Studied by Time-Resolved USAXS and SAXS. *Macromolecules* **2022**, *55*, 684−695.
(68) Amann, M.; Diget, J. S.; Lyngsø, J.; Pedersen, J. S.; Narayanan, T.; Lund, R. Kinetic Pathways for Polyelectrolyte Coacervate Micelle Formation Revealed by Time-Resolved Synchrotron SAXS. *Macromolecules* **2019**, *52*, 8227−8237.
(69) Liu, X.; Haddou, M.; Grillo, I.; Mana, Z.; Chapel, J.-P.; Schatz, C. Early Stage Kinetics of Polyelectrolyte Complex Coacervation Monitored through Stopped-Flow Light Scattering. *Soft Matter* **2016**, *12*, 9030−9038.
(70) Guinier, A.; Fournet, G. *Small-angle Scattering of X-Rays*; John Wiley and Sons: New York, NY, 1955.
(71) Kratky, O.; Porod, G. *Small Angle X-Ray Scattering*; Academic Press: New York, NY, 1982.
(72) Krogstad, D. V. *Investigating the Structure-Property Relationships of Aqueous Self-Assembled Materials*; University of California: Santa Barbara, 2012.
(73) Bian, S.; Zheng, Z.; Liu, Y.; Ruan, C.; Pan, H.; Zhao, X. A Shear-Thinning Adhesive Hydrogel Reinforced by Photo-Initiated Crosslinking as a Fit-to-Shape Tissue Sealant. *J. Mater. Chem. B* **2019**, *7*, 6488−6499.
(74) Townsend, J. M.; Beck, E. C.; Gehrke, S. H.; Berkland, C. J.; Detamore, M. S. Flow behavior prior to crosslinking: The need for precursor rheology for placement of hydrogels in medical applications and for 3D bioprinting. *Prog. Polym. Sci.* **2019**, *91*, 126−140.

https://doi.org/10.1021/acs.macromol.2c00590
Macromolecules 2022, 55, 4481−4491